**Title**
COMPARISONS OF CODED APERTURE IMAGING USING VARIOUS APERTURES AND DECODING METHODS



**Author**
Chang, L.-T.

**Publication Date**
1976-07-01

Peer reviewed

To be presented at the 1976 SPIE Symposium
Applications of Optics in Medicine and
Biology, San Diego, CA,
August 23 - 27, 1976



# COMPARISONS OF CODED APERTURE IMAGING USING VARIOUS APERTURES AND DECODING METHODS

Lee-Tzuu Chang, Burns Macdonald, and
Victor Perez-Mendez



July 1976

Prepared for the U. S. Energy Research and
Development Administration under Contract W-7405-ENG-48



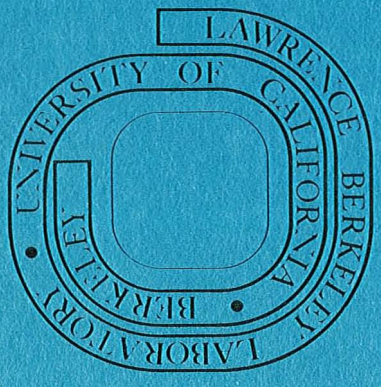

# COMPARISONS OF CODED APERTURE IMAGING USING VARIOUS APERTURES AND DECODING METHODS*

Lee-Tzuu Chang, Burns Macdonald, Victor Perez-Mendez
Lawrence Berkeley Laboratory, University of California
Berkeley, California 94720

## Abstract

The utility of coded aperture imaging of radioisotope distributions in Nuclear Medicine is in its ability to give depth information about a three dimensional source. We have calculated imaging with Fresnel zone plate and multiple pinhole apertures to produce coded shadows and reconstruction of these shadows using correlation, Fresnel diffraction, and Fourier transform deconvolution. Comparisons of the coded apertures and decoding methods are made by evaluating their point response functions both for in-focus and out-of-focus image planes. Background averages and standard deviations were calculated. In some cases, background subtraction was made using combinations of two complementary apertures. Results using deconvolution reconstruction for finite numbers of events are also given.

## Introduction

In Nuclear Medicine imaging a gamma camera with a pinhole aperture or a multichannel parallel collimator gives a simple and direct way to obtain images of radionuclide distributions in the x-y plane. One way to obtain depth information about the source distribution is to take several exposures at different angles with the z axis. Another way that gets these different projections of the source distribution simultaneously is to add more pinholes to a single-pinhole aperture plate of a gamma camera (Fig. 1). In this case, however, the pinhole views impinging on the detector overlap one another, the image of the source distribution is no longer recognizable, and a means of image reconstruction is required. This image is said to be coded by the pattern of the aperture plate and is called a coded image or shadowgram.

Any aperture plate with opening other than a single pinhole is a coded aperture and there are many different code patterns. The Multiple Pinhole Arrays (MPAs) and the Fresnel Zone Plates (FZPs) are the best known. The MPA coded aperture is simply an aperture consisting of a number of pinholes. The random pinhole array, first suggested by Dicke[1] for X-ray astronomy and used for solar X-radiation,[2] consists of a large number of pin-holes randomly distributed having an average transmission of 50% (Fig. 2a).

A second type of MPA is the non-redundant pinhole array and an example of this type is shown in Fig. 2b. The positions of the pinholes of this array are carefully chosen so that the vector distance between any two pinholes occurs only once, i.e., the pinholes are space non-redundantly. This non-redundancy means that the autocorrelation function of this pinhole array, sharply peaked at the center is uniformly distributed elsewhere. References and further information can be found in Ref. 3.

The first use of a coded aperture was by Mertz and Young who used a Fresnel zone plate to image X-ray stars.[4] Barrett later applied this method to Nuclear Medicine imaging.[5] The Fresnel zone plate consists of a number of concentric opaque and transmitting zones and the radius of the nth zone is given by $r_n = \sqrt{n}\, r_1$, where $r_1$ is the first zone radius (Fig. 2c).

## The Coded Shadow and Its Reconstruction

Coded aperture imaging is a two step process where the coded shadow of the object is first obtained and then, from this, tomographic images of transverse planes through the object are then reconstructed (decoded). These tomographic images have a given plane in focus with out-of-focus background from other object planes and, possibly, background from the imaging process superimposed.

### Imaging and Reconstruction

We consider the imaging of a 2-D source distribution first. Let the distribution of the source object be given by $o(\underline{r})$ and the projection of the coded aperture pattern on the detector from a point source at $\underline{r} = \underline{0}$ in the object plane be given by $h(\underline{r})$. Assuming the imaging system is linear and space-invariant, the coded image or shadowgram $s(\underline{r})$ of the object $o(\underline{r})$ on the detector plane is given by a convolution integral,

$$s(\underline{r}) = \frac{1}{\alpha^2}\, o\left(-\frac{1}{\alpha}\,\underline{r}\right) \circledast h(\underline{r}) \qquad (1)$$

where $\alpha = S_o/S_1$ is the magnification of the system with the geometry shown in Fig. 1. $S_1$ is the source to aperture distance and $S_o$ is the aperture to detector distance. The factor $1/\alpha^2$ results from a consideration of the total intensity of the shadowgram.

To obtain the image of $o(\underline{r})$ we have to perform a decoding operation on the shadowgram $s(\underline{r})$. The decoding operation can be expressed in a form of convolution. If we use $h'(\underline{r})$ to represent the impulse response of the reconstruction system the resulting image $i(\underline{r})$ of the reconstruction of shadowgram $\alpha^2 s(-\alpha r)$ is then given by

$$i(\underline{r}) = \alpha^2 \, s(-\alpha\underline{r}) \circledast h'(\alpha\underline{r}) = o(\underline{r}) \circledast [h(-\alpha\underline{r}) \circledast h'(\alpha\underline{r})] \tag{2}$$

The point response of the entire process (imaging and reconstruction), found when $o(\underline{r})$ is a delta function, is

$$p(\underline{r}) = h(-\alpha\underline{r}) \circledast h'(\alpha\underline{r}) \tag{3}$$

For an extended source distribution $o(\underline{r})$ the reconstructed image $i(\underline{r})$ is

$$i(\underline{r}) = o(\underline{r}) \circledast p(\underline{r}) \tag{4}$$

Decoding Methods

The following methods of shadowgram reconstruction have been used in this paper.

1. Correlation. This commonly employed method uses the same aperture function for reconstruction as it does for the shadowgram exposure. Equation 3 for the reconstruction of a point source by this method becomes

$$p(\underline{r}) = h(-\alpha\underline{r}) \circledast h(\alpha\underline{r}) = h(\alpha\underline{r}) \otimes h(\alpha\underline{r}) = a(\alpha\underline{r}) \tag{5}$$

where $\otimes$ is used to represent the correlation of two functions and $a(\underline{r})$ is defined as the autocorrelation function of $h(\underline{r})$. The reconstructed image of an extended object $o(\underline{r})$ by this method is therefore given by $i(\underline{r}) = o(\underline{r}) \circledast a(\alpha\underline{r})$.

2. Fresnel Diffraction. The focussing properties for light of the Fresnel zone plate, unique among coded apertures, have often been used for the reconstruction of FZP coded shadowgrams. The transmission function of the zone plate can be expressed in a complex Fourier series as

$$h_{zp}(\underline{r}) = \left[ 1/2 \pm \sum_{\substack{n \\ \text{odd}}} \frac{i}{n\pi} e^{in\pi r^2/r_1^2} \right] \text{circ}(\underline{r}/r_N) \tag{6}$$

The negative sign is for a positive zone plate (center transparent) and the positive sign is for a negative zone plate (center opaque). $r_N$ is the radius of the zone plate. Using Fresnel diffraction we may express the diffracted amplitude $g(\underline{r})$, at a distance z downstream from a zone plate illuminated by a plane wave of amplitude 1 and wavelength $\lambda$, as a convolution,[6]

$$g(\underline{r}) = h_{zp}(\underline{r}) \circledast w(\underline{r}) \, , \tag{7}$$

omitting a constant phase factor. $w(\underline{r})$ is the Fresnel wavefunction.

$$w(\underline{r}) = - \frac{i}{\lambda z} e^{i\pi r^2/\lambda z} \tag{8}$$

The focal plane is located at $z = r_1^2/\lambda$. The reconstructed image (amplitude distribution) of an extended object $o(\underline{r})$ by this system is given by $i(\underline{r}) = o(\underline{r}) \circledast g(\underline{r})$.

3. Fourier Transform Deconvolution. Taking the Fourier transform of Eq. (2) and omitting the scale factor $\alpha$ we have $I(\underline{\nu}) = O(\underline{\nu}) \, H^*(\underline{\nu}) \, H'(\underline{\nu})$. We can determine the spatial frequency components of the object at frequencies where $|H(\underline{\nu})|$ is not zero by letting $H'(\underline{\nu}) = 1/H^*(\underline{\nu}) = H(\underline{\nu})/|H(\underline{\nu})|^2$. One would like to avoid excessive amplification of noise in the shadowgram when $|H(\underline{\nu})|$ is close to zero. One approach, taken by Wilson, Parker and Dance for the zone plate, is to make the following choice for $H'(\underline{\nu})$.[7]

$$H'(\underline{\nu}) = H(\underline{\nu}) / |H(\underline{\nu})|^2 , \quad \text{if } |H(\underline{\nu})| > \beta H_{max}$$

$$H'(\underline{\nu}) = H(\underline{\nu}) / \beta^2 H_{max}^2 , \quad \text{if } |H(\underline{\nu})| \leq \beta H_{max} \tag{9}$$

where $H_{max}$ is the largest Fourier frequency component of $|H(\underline{\nu})|$, and $\beta$ is a variable parameter which is chosen to optimize the resolution (for small $\beta$) and the signal to noise (for larger $\beta$) of the system.

Complex Coded Aperture Imaging

If $h^+(\underline{r})$ is the transmission function of a binary (0 or 1) code pattern with 50% transmission we may define its complementary pattern $h^-(\underline{r})$ by interchanging the 0's and 1's in $h^+(\underline{r})$ within the code pattern boundary.

We can form two shadowgrams $s^+(\underline{r})$ and $s^-(\underline{r})$ of a source object $o(\underline{r})$ with a fixed imaging geometry, $s^+(\underline{r})$ from code pattern $h^+(\underline{r})$ and $s^-(\underline{r})$ from the complement $h^-(\underline{r})$. The difference of the two shadowgrams, $s(\underline{r}) = s^+(\underline{r}) - s^-(\underline{r})$, is equivalent to the shadowgram formed directly from imaging $o(\underline{r})$ with a code pattern $h(\underline{r}) = h^+(\underline{r}) - h^-(\underline{r})$.

$$s(\underline{r}) = s^+(\underline{r}) - s^-(\underline{r}) = o(\underline{r}) \circledast [h^+(\underline{r}) - h^-(\underline{r})] \tag{10}$$

Thus, a coded aperture imaging system with two or more different apertures can produce an effective coding function $h(\underline{r})$ which can have negative values and not just the two physically possible values, 0 or 1. Examples are a positive and a negative zone plate, and a random pinhole array and its complementary array.

Imaging of a Three Dimensional Source Distribution

We represent a 3-D object distribution by $N_p$ planes $o_i(\underline{r})$, $i = 1,\ldots N_p$, separated by the depth resolution of the system. The distance between object plane $o_i$ and the aperture plate is $S_i$. The aperture to detector distance is $S_o$. We can formulate an expression for the shadowgram of this object distribution, similar to Eq. (1).

$$s(\underline{r}) = \sum_{i=1}^{N_p} \frac{1}{\alpha_i^2} o_i\left(-\frac{1}{\alpha_i}\underline{r}\right) \circledast h_i(\underline{r}) \tag{11}$$

where $h_j(\underline{r})$ is the point response of the detector to a point source at $\underline{r} = \underline{o}$ of object plane i, and $\alpha_i = S_o/S_i$. The image $i_j(\underline{r})$, having the jth plane in focus, can be formed from $s(\underline{r})$ by convolving it with the reconstruction function $h'(\underline{r})$ in the following way.

$$i_j(\underline{r}) = \alpha_j^2 \, s(-\alpha_j\underline{r}) \circledast h_j'(\alpha_j\underline{r}) = o_j(\underline{r}) \circledast h_j(-\alpha_j\underline{r}) \circledast h_j'(\alpha_j\underline{r})$$

$$+ \sum_{i \neq j}^{N_p} \frac{\alpha_j^2}{\alpha_i^2} o_i\left(\frac{\alpha_j}{\alpha_i}\underline{r}\right) \circledast h_i(-\alpha_j\underline{r}) \circledast h_j'(\alpha_j\underline{r}) \tag{12}$$

The first term on the right side of Eq. (12) is the in-focus plane $o_j(\underline{r})$ (see Eq. 2) and the second term comes from all the out-of-focus planes $o_i$, $i \neq j$. If the image is reconstructed by the correlation method $i_j(\underline{r})$ can be expressed as

$$i_j(\underline{r}) = o_j(\underline{r}) \circledast a_j(\alpha_j\underline{r}) + \sum_{i \neq j}^{N_p} \frac{\alpha_j^2}{\alpha_i^2} o_i\left(\frac{\alpha_j}{\alpha_i}\underline{r}\right) \circledast c_{ij}(\alpha_j\underline{r}) , \tag{13}$$

where the autocorrelation function $a_j(\alpha_j\underline{r})$ is $h_j(-\alpha_j\underline{r}) \circledast h_j(\alpha_j\underline{r})$ and the crosscorrelation functions $c_{ij}(\alpha_j\underline{r})$ are $h_i(-\alpha_j\underline{r}) \circledast h_j(\alpha_j\underline{r})$.

Results

A useful way to make comparisons between various coded apertures and decoding methods is to compare their point responses since these depend only on the system and not on the object. For a linear and space-

invariant imaging system the response of the system to an extended source distribution is completely determined by the system's in-focus and out-of-focus point responses (Eqs. 12 and 13).

We have made a number of computer simulations of coded aperture imaging using various coded apertures and decoding methods. The coded apertures are of similar size and spatial resolution, and were exposed in the same geometries. The apertures used are:

1) A negative zone plate with transmission function $h^-_{zp}(\underline{r})$. The zone plate has 10 zones and the width of the last annular zone is 2.5 mm. The diameter of the zone plate is 95 mm.

2) A composite zone plate with transmission function $h^+_{zp}(\underline{r}) - h^-_{zp}(\underline{r})$. $h^-_{zp}(\underline{r})$ is as given above. $h^+_{zp}(\underline{r})$ is the positive zone plate which has the same number of transparent rings and the same first zone radius.

3) A random pinhole array with transmission function given by $h^+_{rp}(\underline{r})$.

This array is generated randomly on a grid of 38×38 elements with half of the elements occupied by the pinholes. The size of the array is 95 mm and the size of each pinhole in the array is 2.5 mm.

4) A composite random pinhole array with transmission function given by $h^+_{rp}(\underline{r}) - h^-_{rp}(\underline{r})$. $h^-_{rp}(\underline{r})$ is the array complementary to $h^+_{rp}(\underline{r})$ given above.

5) A non-redundant pinhole array with transmission function $h_{nr}(\underline{r})$. This nine hole array (Fig. 2b) has a maximum diameter of 95 mm with pinholes 2.5 mm in diameter.

6) A regular pinhole array, transmission function $h_{rg}(\underline{r})$. This array, having the same size, number of pinholes, and pinhole diameter as the non-redundant array, is arranged in a 3 by 3 regular pattern. In all our computer simulations a single point source located at $S_1$ = 20 cm was reconstructed, from its shadowgram, on two planes, $S_1$ = 20 cm and $S_2$ = 25 cm. Aperture to detector distance was $S_p$ = 39 cm. Thus, the in-focus point response plane is obtained as is also the response of the system for an out-of-focus plane (Fig. 3). The functions are all normalized to one for the in-focus peak. For the diffraction and deconvolution methods the image space pictured is a 480 mm square. For the correlation method it is a 570 mm square. The negative zone plate responses (Fig. 3g) are plotted inverted since the central peak is negative. The calculations for diffraction reconstructions are based on the real parts of their diffracted amplitudes.

To evaluate the quality of the imaging systems considered we have tabulated the average background and the background standard deviation for each image (Table 1). These quantities are calculated over an area 480 mm in diameter. For the in-focus plane the area does not include the central peak. One should not judge image quality just on the basis of low background fluctuations since subsidiary peaks in the point response functions will give rise to artifacts when extended objects are imaged. When imaging objects spread over a number of planes in depth, the out-of-focus background fluctuations are more important than the in-focus values since all other object planes contribute to a given in-focus plane.

The point responses of Fig. 3 were generated without quantum noise, that is, with no statistical fluctuations of the positions of the events composing the shadowgram. Since the deconvolution method is expected to be sensitive to quantum noise we have also made these reconstructions using statistical shadowgrams (Fig. 4 and Table 1). Results with several values of the parameter $\beta$ were compared and the ones with lowest background fluctuations were chosen. The numbers of events for the different apertures corresponded roughly to using the same intensity source. The cases for the regular and the non-redundant arrays used an average of 25 events/pinhole. The random array used 16 events/pinhole and composite random array imaging used 16 events/pinhole for each array. The negative zone plate collected 16 events for an equivalent area (a one resolution length square).

## Conclusions

The calculated point response functions give a detailed picture of the coded aperture systems studied, exhibiting well-known properties of these systems as well as features not as well known. With correlation decoding these functions for the negative zone plate and the random pinhole array show the unacceptably large background expected from high transmission apertures (50%). This background is eliminated when composite imaging is used with the complementary apertures. Subsidiary peaks in the in-focus and out-of-focus planes can be expected to give artifacts in extended source imaging. The results for the regular array show why this system is unacceptable. The best results for correlation decoding are for the composite random pinhole array where the out-of-focus response function is uniformly spread out, with small standard deviation and without salient spikes.

Diffraction decoding, only possible with the Fresnel zone plate, shows for the single zone plate a fairly high average background which, of course, disappears with the composite zone plate. For all decoding methods used here, single and composite Fresnel zone plate apertures show an intense central ring in the out-of-focus plane. Thus, zone plate imaging can be expected to have artifact problems that the random pinhole array would not have.

Decoding by deconvolution generally gave the smallest in-focus background fluctuations. The out-of-focus plane fluctuations do not increase very much when a finite number of events is used, although the in-focus plane fluctuations do. The non-redundant array has a number of peaks in the out-of-focus plane making that aperture less attractive than the two random pinhole arrays which have small background fluctuations and the smoothest out-of-focus point responses obtained with this method. This decoding depends on the extent of zeroes in the transfer function. Of the apertures studied here the zone plate has the largest number of small values[8] and the largest fluctuations in the response function with this method are obtained with this aperture. The deconvolution method merits further study. Our choices of $\beta$ were not exhaustive and the point response function representation does not exhibit directly the effect of altered spatial frequencies.

From a comparison of the point response functions presented here it would appear that the best extended source imaging would be with the composite random pinhole aperture with correlation decoding. The in-focus and out-of-focus backgrounds are uniformly spread out with the lowest fluctuations, having no subsidiary peaks. The single and composite random arrays with deconvolution decoding have similar properties but their out-of-focus noise is somewhat larger.

## References


1. Dicke, R. H., "Scatter-Hole Cameras for X-Rays and Gamma-Rays," Astrophysical J., Vol. 153, L101, Aug. 1968.
2. Blake, R. L., A. J. Burek, E. Fenimore, and R. Puetter, "Solar X-Ray Photography with Multiplex Pinhole Camera," Rev. Sci. Instrum., Vol. 45, n.4, p. 513, 1974.
3. Chang, L. T., B. Macdonald, V. Perez-Mendez, and L. Shiraishi, IEEE Trans. Nucl. Sci. NS-22, 374 (1975).
4. Mertz, L. and N. O. Young, "Fresnel Transformations of Images", Proc. Int. Conf. on Opt. Inst., London, p. 305, 1961.
5. Barrett, H. H., "Fresnel Zone Plate Imaging in Nuclear Medicine," J. Nucl. Med., Vol. 13, n. 6, p. 382, 1972.
6. Winthrop, J. T. and C. R. Worthington, "Convolution Formulation of Fresnel Diffraction," J. Opt. Soci. Am., Vol. 56, n. 5, p. 588, 1964.
7. Dance, D. R., B. C. Wilson, and R. P. Parker, "Digital Reconstruction of Point Sources Imaged by a Zone Plate Camera," Phys. Med. Biol., Vol. 20, n. 5, p. 747, 1975.
8. Chang, L. T., "Redionuclide Imaging with Coded Apertures and Three Dimensional Image Reconstructions from Focal Plane Tomography," Ph.D. Thesis, Lawrence Berkeley Laboratory Report LBL 4887, May, 1976.


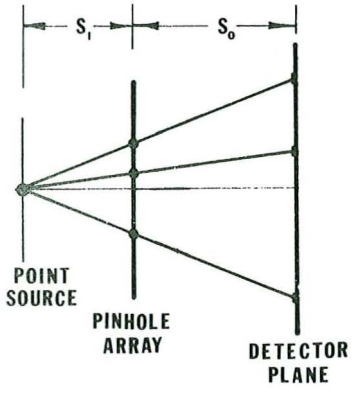


Fig. 1. Illustration of Coded Aperture Imaging - Formation of Coded Image.

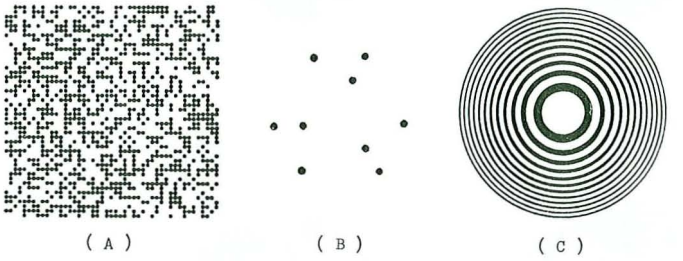


Fig. 2. Examples of Coded Aperture Patterns. (a) Random pinhole array (b) Nonredundant pinhole array (c) Fresnel zone plate.

* This work has been supported by the U. S. Atomic Energy Commission and by the National Institutes of General Medical Services of the National Institutes of Health, Fellowship #1F03GM57292-01, and Grant #GM21017.

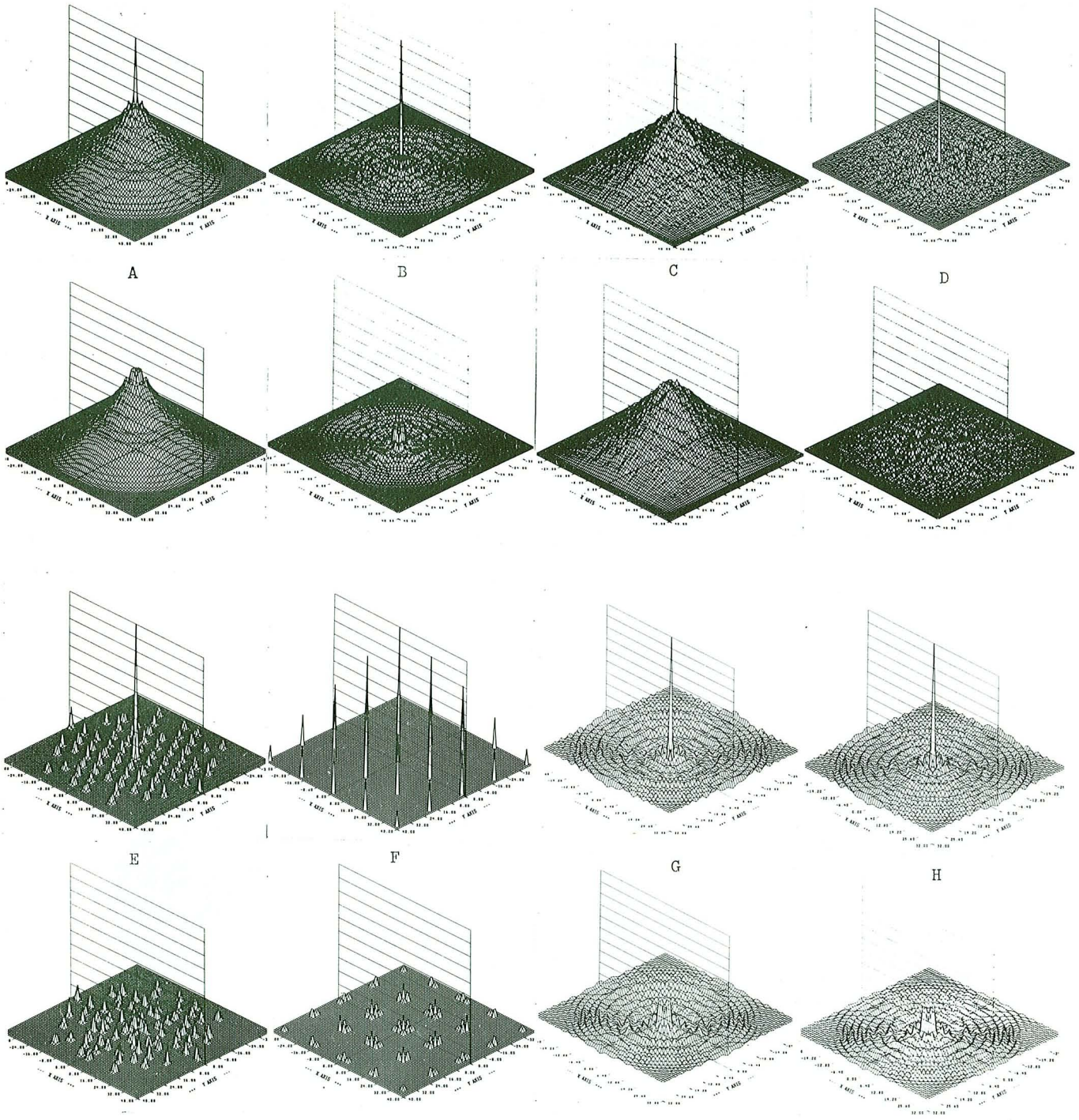


Fig. 3. Plots of the Point Responses of Various Coded Aperture Systems. No quantum noise. The top half of each pair is the in-focus point response, the bottom half is the out-of-focus point response. The apertures and decoding methods used for generating these plots are listed in Table 1.

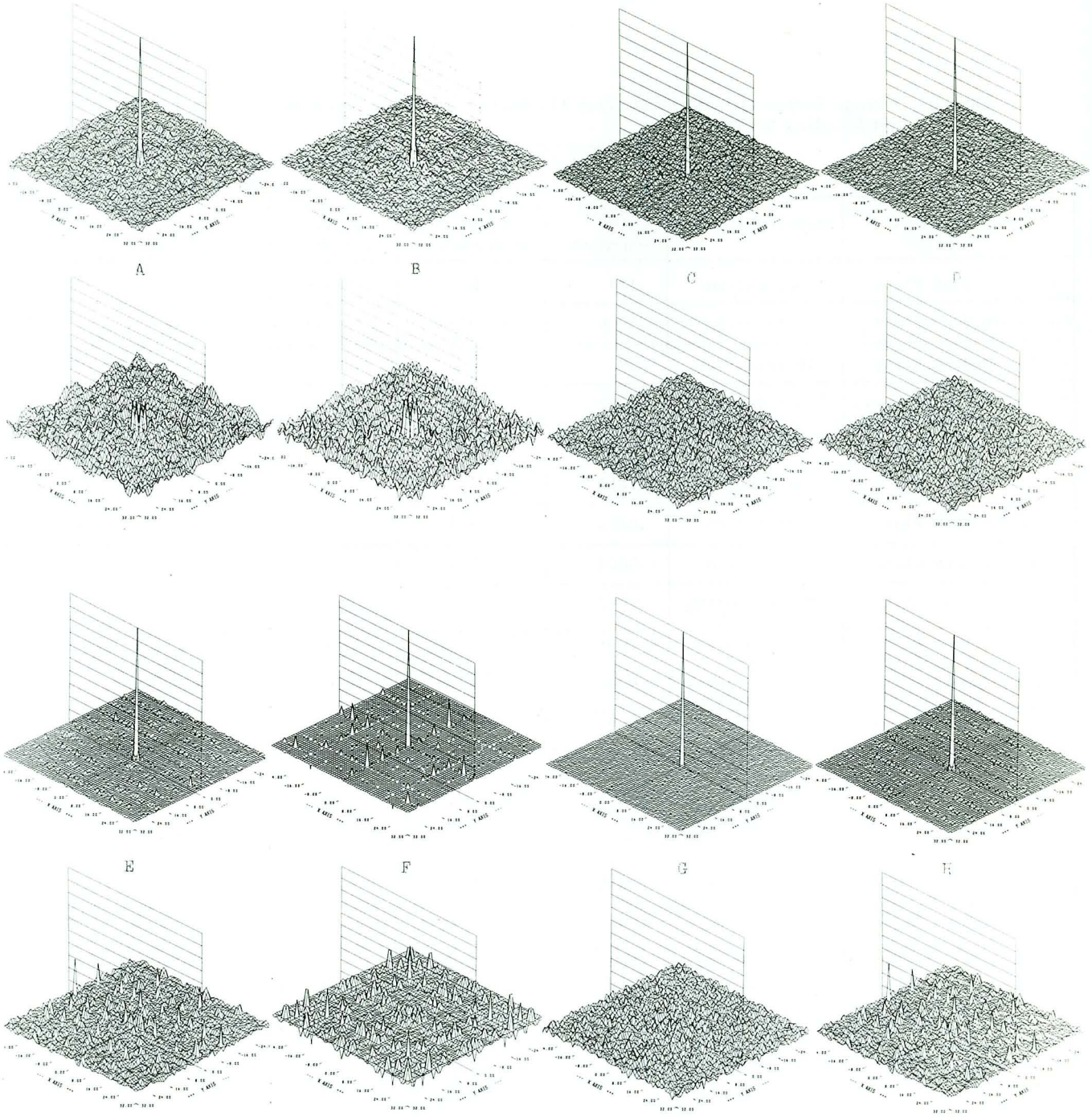


Fig. 4. Plots of the Point Responses with Deconvolution. With and without quantum noise. The apertures used and the gamma-ray events collected for generating these plots are listed in Table 1. The point responses are shown in the same way as in Fig. 3.

Table 1. Average Background and Background Fluctuation of Point Responses for Various Apertures and Decoding Methods.

| Coded Apertures | Decoding Methods | Average Background | | Background Fluctuation | | Illustration of the Point Responses |
|---|---|---|---|---|---|---|
| | | In-Focus Point Responses | Out-of-Focus Point Responses | In-Focus Point Responses | Out-of-Focus Point Responses | |
| Negative Zone Plate | Correlation | .183 | .189 | .1036 | .1229 | Fig. 3A |
| Composite Zone Plate | Correlation | -.0006 | -.0000 | .0181 | .0166 | Fig. 3B |
| Random Pinhole Array | Correlation | .201 | .211 | .0953 | .1123 | Fig. 3C |
| Composite Random Array | Correlation | .0002 | .0004 | .0168 | .0143 | Fig. 3D |
| Non-Redundant Array | Correlation | .0053 | .0066 | .0194 | .0198 | Fig. 3E |
| Regular Array | Correlation | .0014 | .0017 | .0283 | .0097 | Fig. 3F |
| Negative Zone Plate | Diffraction | .0222 | .0215 | .0317 | .0353 | Fig. 3G |
| Composite Zone Plate | Diffraction | -.0004 | .0004 | .0164 | .0212 | Fig. 3H |
| Negative Zone Plate | Deconvolution $\beta = 0.01$ | -.0002 | .0003 | .0053 | .0226 | |
| Composite Zone Plate | Deconvolution $\beta = 0.1$ | -.0001 | -.0006 | .0052 | .0308 | |
| Random Pinhole Array | Deconvolution $\beta = 0.01$ | .0000 | .0003 | .0035 | .0197 | |
| Composite Random Array | Deconvolution $\beta = 0.1$ | -.0003 | -.0001 | .0026 | .0205 | Fig. 4G |
| Non-Redundant Array | Deconvolution $\beta = 0.1$ | -.0000 | -.0006 | .0042 | .0214 | Fig. 4H |
| Regular Array | Deconvolution $\beta = 0.1$ | .0003 | .0005 | .0100 | .0238 | |
| Imaging of Point Gamma-Ray Source with Finite Photon Emission, by Deconvolution. | | | | | | |
| Negative Zone Plate | 10,000 Events $\beta = 0.01$ | -.0003 | .0004 | .0147 | .034 | Fig. 4A |
| Composite Zone Plate | 20,000 Events $\beta = 0.1$ | -.0007 | -.0004 | .0124 | .0367 | Fig. 4B |
| Random Pinhole Array | 11,500 Events $\beta = 0.01$ | .0000 | .0003 | .0089 | .0209 | Fig. 4C |
| Composite Random Array | 23,000 Events $\beta = 0.1$ | -.0003 | -.0001 | .0069 | .0209 | Fig. 4D |
| Non-Redundant Array | 225 Events $\beta = 0.1$ | .0000 | .0006 | .0051 | .0213 | Fig. 4E |
| Regular Array | 225 Events $\beta = 0.1$ | .0003 | .0006 | .0112 | .0243 | Fig. 4F |